A FAST RADIATIVE TRANSFER MODEL FOR SIMULATING RADIANCES OF THE STRATOSPHERIC WIND INTERFEROMETER FOR TRANSPORT STUDIES SATELLITE INSTRUMENT.

D.S. Turner and Y.J. Rochon

Atmospheric Science & Technology Directorate, Environment Canada

ABSTRACT

A fast radiative transfer model to simulate the limb infrared radiances for the Stratospheric Wind Interferometer for Transport Studies (SWIFT) satellite instrument, a Doppler Michelson interferometer, has been developed. The model referred to as RT-SWIFT is designed to simulate the four points of the instrument's interferogram required to retrieve the wind-induced phase shifts of the spectra in the vicinity of the 1133.4335(cm^{-1}) ozone line. The development of the model involved the creation of an accurate line-by-line transmittance/radiance database, selection of suitable predictors for the gases and, the wind, planetary rotation and satellite velocities, and the creation of regression coefficients. The assessment of the model relies on evaluating the associated accuracy of the derived radiances and of the recovered the line of sight Doppler wind using a set of atmospheric states. The preliminary intensity error levels of the fast radiative transfer model are within 4% for tangent heights in the 20-50km range. The most novel aspect of the model is a representation of the sensitivity to Doppler wind. The line of sight Doppler wind error level contributions from the current model are within 4-5m/s. Further investigation would be required to determine the level of impact of optimization on reducing wind error levels.

INTRODUCTION

With the exception of a sparse global radio-sonde network, there are no direct stratospheric wind measurements used in assimilation. The lack of wind measurements is a limiting factor to the quality of stratospheric analyses and forecasts, particularly in the tropics. SWIFT is to address these inadequacies by providing globally distributed stratospheric wind profiles on a daily basis. Figure 1 provides an estimate of the possible impact of SWIFT winds. SWIFT measurements can also be used to study chemical transport and ozone fluxes from co-located wind and ozone measurements.

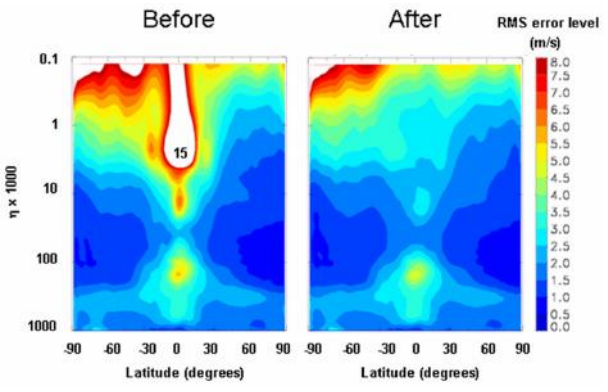

Figure 1: **Reduction of zonal wind component RMS analysis error levels from the assimilation of SWIFT winds. Zonally averaged RMS error levels are depicted for September from results of 3-D data assimilation OSSEs without (before) and with (after) use of simulated SWIFT winds conducted using the GEM-BACH model. (Rochon et al, 2008 Fall AGU; see also Lahoz et al, 2005, for additional examples)**

In order for the measurements to be useful in near real time assimilation, a fast forward radiative transfer model (henceforth designated RT-SWIFT) is required to simulate the instrument's response and must be sufficiently accurate for the assimilation of SWIFT observations to yield positive impact on the analyses and forecasts. This article discusses the development and testing of RT-SWIFT for simulating the measured SWIFT four-point interferogram and the subsequent derivation of a Doppler line-of-sight wind profile.

MEASUREMENT CONCEPT

In order to measure the Doppler shift induced by the atmospheric winds, the emission from an isolated spectral line is projected through a field-widened Michelson interferometer from which an interferogram is obtained. Figure 2 is a representative 4-point interferogram of one of 6561 pixels on the detector array, each of which correspond to a limb view. SWIFT measures the line of sight (LOS) winds in two directions, fore and aft which allows for a vertical wind recovery.

For low order fringes —small optical path differences (OPD)— a Doppler shift induces an extremely small shift (ie, stretching or compression) of the interferogram, producing a difference with the un-shifted interferogram. At larger OPDs this difference of phase shift relative to the un-shifted interferogram increases.

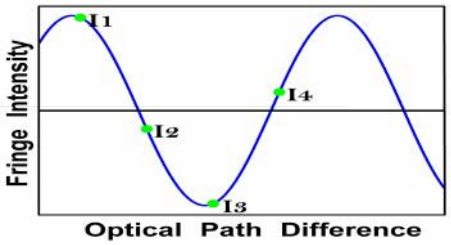

Figure 2: **Four point measurement of a pixel interferogram. Every pixel on the detector array has a similar interferogram associated with it.**

The atmospheric winds introduce a Doppler shift to the atmospheric emission lines in the direction towards the instrument. The phase shift is related to the OPD, wavenumber and wind speed by

$$\varphi^{w} = 2\pi\Delta_{o}\tilde{\nu}\frac{w}{c} \qquad (1)$$

This shift is very small compared to an interferogram where there are no winds –the zero-wind interferogram. For a wind of 1m/s and an OPD of 1cm the shift is an undetectable value of 1/265,000th of a fringe. For an OPD of 16cm the shift becomes manageable at 1/16,500th of a fringe.

The final interferogram is a superposition of many interferograms due to various emission lines and winds from various points along the LOS and is equivalent to that of a single spectral line and is represented as (Shepherd et al, 1993)

$$I_{i} = I_{o}\left[1 + UV\cos(\Phi + \varphi_{i})\right] \qquad (2)$$

Equation 2 can be reformed as a truncated Fourier series and solved for Φ^{s} given four measured points (see fig. 2):

$$\Phi = \tan^{-1}\left(\frac{(I_4 - I_2)[\cos(\varphi_1) - \cos(\varphi_3)] - (I_1 - I_3)[\cos(\varphi_4) - \cos(\varphi_2)]}{(I_4 - I_2)[\sin(\varphi_1) - \sin(\varphi_3)] - (I_1 - I_3)[\sin(\varphi_4) - \sin(\varphi_2)]}\right) \qquad (3)$$

A more complete description of the instrument can be found in Rahnama et al, 2006.

RADIATIVE TRANSFER

The four measurement points of figure 2 are simulated by

$$I_i = \int \int_{\infty}^{o} \Im_i(\tilde{\nu})\, B(\tilde{\nu}, T(s))\, \frac{\partial \Im(\tilde{\nu}, s)}{\partial s}\, ds\, d\tilde{\nu} \qquad (4)$$

where $\Im_i(\tilde{\nu}) = \tau_i^{opt}(\tilde{\nu})[1 + U\cos(2\pi\Delta\tilde{\nu})]$

Equation 4 can be approximated by

$$I_i \approx \sum_{k=2}^{N} (\langle \Im_{ik-1} \rangle - \langle \Im_{ik} \rangle) \langle B_{ik} \rangle \qquad (5)$$

where $\langle \Im_k \rangle$ is the mean transmittance from the k^{th} cell to the satellite and $\langle B_k \rangle$ is the mean Planck function for the k^{th} cell and the brackets indicate spectral averaging,

$$\langle F \rangle = \frac{\int \Im(\tilde{\nu})\, F(\tilde{\nu})\, d\tilde{\nu}}{\int \Im(\tilde{\nu})\, d\tilde{\nu}}$$

Equation 4 is the instrument simulation equation used by a line-by-line model applied in developing the fast forward model and equation 5 is the basis of the fast forward model.

RT-SWIFT

At the onset of the RT-SWIFT development a target upper bound of 1m/s was proposed for the RT-SWIFT wind error level contribution. For the purposes of this study only the instrument fore-view and central column of the detector array is considered.

Transmittance Model, $\langle \Im(s) \rangle$

The RT-SWIFT transmittance model is very similar to that of RT-MIPAS (Bormann et al, 2005). It is set on 100 constant p-levels (RTTOV-9, Saunders et al, 2008) of which 33 are defined to be the tangent pressures (.71mb to 77.2mb) of the limb paths considered, hence 33 models (ie, the same model with different coefficients) are developed. The vertical distribution of modelled limb paths do not necessarily coincide with instrument views, but it is assumed that they can be interpolated to actual views (Turner et al, 2008)

The transmittance of the absorbing atmosphere is modelled using the formulation of McMillin et al. (1995)

$$\langle \Im_k \rangle = \langle \Im_k^{O_3} \rangle \frac{\langle \Im_k^{O_3 + N_2O} \rangle}{\langle \Im_k^{O_3} \rangle} \frac{\langle \Im_k^{O_3 + N_2O + H_2O} \rangle}{\langle \Im_k^{O_3 + N_2O} \rangle} \frac{\langle \Im_k^{O_3 + N_2O + H_2O + fg} \rangle}{\langle \Im_k^{O_3 + N_2O + H_2O} \rangle}$$

$$= \langle {}^{eff}\Im^{O_3} \rangle \langle {}^{eff}\Im^{H_2O} \rangle \langle {}^{eff}\Im^{N_2O} \rangle \langle {}^{eff}\Im^{fg} \rangle \qquad (6)$$

where *fg* represents the contributions of the so-called fixed gases.

The transmittance from a point *j* on the limb path to the observer can be defined in terms of optical depth, X_j

$$\langle \Im_j \rangle = e^{-X_j} \qquad (7)$$

The effective optical depth is represented by a regression model for a series of atmospheric cells that start at the observer and works its way across to the far side of the limb path.

$$\mathbf{X}_k = \mathbf{X}_{k-1} + ({}^{eff}\chi_k^{O_3} + {}^{eff}\chi_k^{H_2O} + {}^{eff}\chi_k^{N_2O} + {}^{eff}\chi_k^{fg}) \chi_k^{osr} \chi_k^{vsr} \quad (8)$$

where the additional terms χ^{osr} and χ^{vsr} have been added to account for the change in the optical depth caused by the LOS satellite and planetary rotational speed, and the LOS atmospheric winds, respectively.

Each χ_k term in Eq(8) is a sum of predictors, $x_{\ell k}$, and coefficients, $a_{\ell k}$, of the form

$$\sum_{\ell=1} a_{\ell k} x_{\ell k} \quad (9)$$

The predictors for O_3, H_2O and *fg* (fixed gases) can be found in tables 3 and 4 of Bormann et al (2005). The N_2O predictors are the same as the O_3 predictors with the O_3 volume mixing ratio being replaced by the N_2O counterpart. The fixed gases (constant profiles) consist of the absorbers CH_4, SO_2, NH_3, CFC-12 and CFC-22. The coefficients are evaluated assuming a constant satellite and Earth rotational speed without the addition of the atmospheric wind. The coefficients depicting the sensitivity to atmospheric wind are obtained afterwards. The new predictors for χ^{osr} and χ^{vsr} are listed in table 1.

	χ^{osr}	χ^{vsr}
1	$v_j^{sr} - {}^{ref}v_j^{sr}$	$\frac{1}{2}(v_{j-1}^{LOS} + v_j^{LOS})$
2	$(v_j^{sr} - {}^{ref}v_j^{sr})^2$	$\frac{\sum_{k=1}^{j} \tilde{P}_k (v_{k-1}^{LOS} + v_k^{LOS}) \delta s_k}{\sum_{k=1}^{j} \tilde{P}_k \bar{Z}_k^{ref}}$
3	$(v_j^{sr} - {}^{ref}v_j^{sr})^3$	

Table 1: **The predictors required to account for the effect of the LOS satellite plus planetary rotational speed, v_j^{sr}, and LOS atmospheric winds, v^{LOS}. δs, $\bar{Z}^{ref}$ and $\tilde{P}$ are defined in Bormann et al (2005).**

The regression coefficients for each section of Eq(8) are determined by multiple regression using a dependent set of 94 atmospheres (see below).

Planck Function, 〈 B(T) 〉

The planck function is approximated in a manner similar to that described by Planet et al (1988). However instead of a linear relationship between temperature and effective temperature, a cubic relationship is used.

$$\langle B(T) \rangle \approx B(\tilde{\nu}_o, T_{eff}) = \frac{c_1 \tilde{\nu}_o^3}{e^{c_2 \tilde{\nu}_o T_{eff}^{-1}} - 1} \quad (10)$$

where $T_{eff} = a + bT + cT^2 + dT^3$. a, b, c, d and $\tilde{\nu}_o$ are collectively referred to as the band correction coefficients.

It was found that a global function over all limb paths resulted in significant errors, but minimal errors occurred (< .1K) when each limb path was considered independently.

TRAINING AND INDEPENDENT SETS

In order to determine the RT-SWIFT coefficients and to evaluate the resulting regression results, it is necessary to have two training sets, a dependent set for training (coefficient determination) and an independent set for testing. Both sets are extracted from a database constructed from the output of the CMAM-DAS (Polavarapu et al, 2005). This database supplies z, p, T, O_3, N_2O, H_2O, CH_4, CFC-12 and wind profiles for over 100,000 atmospheres. The SO_2, NH_3 and CFC-22 are climatological.

A training set of 94 atmospheres was determined by reducing the 100K+ atmospheres using principle component analysis. Simulated four point interferograms were determined from these atmospheres using a fast line-by-line radiative transfer model (FLBL, Turner, 1995) for a wide range of satellite and Earth rotation velocities assuming SWIFT's response functions for the central column of pixels. The instrument views (tangent heights) were invariant. In addition the transmittances required for determining the RT-SWIFT coefficients are also evaluated.

The independent set consists of 250 independent atmospheres randomly extracted from CMAM-DAS and randomly assigned orbital positions from a set of 104 positions covering 2 orbits assuming a satellite altitude of 650km (C.S. Haley, York University, Toronto, Canada.). As before, four point interferograms are simulated for each position via the FLBL.

In addition to simulating on-orbit interferograms it was also necessary to simulate the interferograms assuming no winds, the zero-wind intensities.

DEPENDENT SET COMPARISON

Figure 5 compares the FLBL simulations with the RT-SWIFT simulations of the training set, ie, the "FLBL minus RT-SWIFT" residuals. Differences result from only the limitations of the RT-SWIFT model as no other error sources have been introduced. A systematic bias exists for intensities but is minimized after differencing to obtain Φ. The biases for Φ_s and Φ_o are about .02° (1/18,1000 of a fringe) and their respective standard deviations are about .02°. The wind phase bias is about .005° with the standard deviation ranging from .04° to .12°. The LOS residual wind biases are less than .4m/s and the standard deviations range from 1.8m/s to 5.2m/s.

LOS-WIND RETRIEVAL

The previous section gives an estimate of the errors in obtaining the LOS winds (equivalent wind from all contributing winds along the path), but not an estimate of the LOS winds at each model level. The simple iterative onion peeling algorithm is applied to obtain the obtain LOS winds for each level (coincident with the tangent height). It was first used with all the variables taken as known, except the winds.

Figure 6 compares the LOS wind profiles applied to the FLBL (ie, the *true* wind profiles) and those retrieved from onion peeling inversions using RT-SWIFT. The biases are less than .5m/s for altitudes greater than 28km and less than 1m/s for altitudes greater than 23m/s. The inversion results below 23km are not as reliable and are often accompanied by significant outliers.

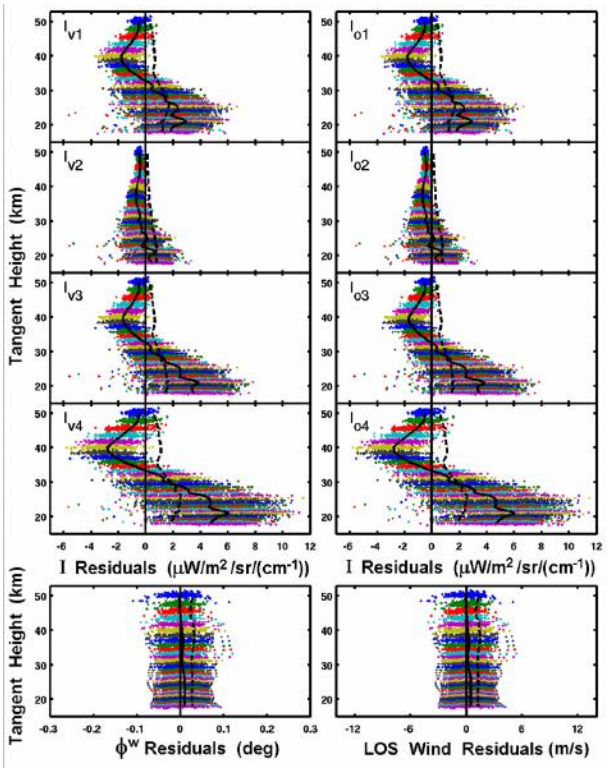

Figure 5: **The residuals of the training set ●, their biases (——) and standard deviations (- - -) for each of the mirror steps, with wind (left) and without wind (right). The two bottom panels show the residuals of the wind phase (left) and the Doppler wind (right). Each horizontal band of colour represents a limb path and the thickness of a band indicates the variability of the tangent heights for each given tangent pressure.**

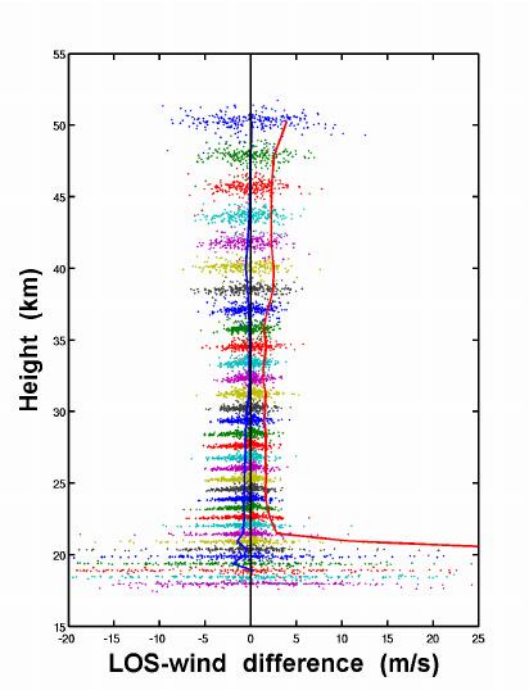

Figure 6: **Residuals between the true LOS-wind and the retrieved LOS-wind ●. The biases (——) and standard deviations (——) are shown. The colourations of ● have the same meaning as in figure 5.**

O_3 and LOS-WIND RETRIEVAL

It is possible to retrieve an ozone profile from the average values of I_1, I_2, I_3, and I_4. As before, a top-down iterative onion peeling algorithm is also used to obtain O_3, this followed by the inversion for the wind. Here, all variables are known except for O_3 and wind.

Figure 7 compares the *true* and retrieved O_3 profiles. The biases vary from .5 to -2ppmv (6 to 12%) above 24km and the standard deviations are less than 1ppmv above 24km. The retrieval for ozone breaks down below 23km due to the current RT-SWIFT limitations with the imposed maximum number of iterations being reached. Comparing figure 6 and the right-most box of figure 7, the added errors due to the O_3 retrieval do not noticeably affect the errors above 25km, but become more significant below where O_3 results are not reliable.

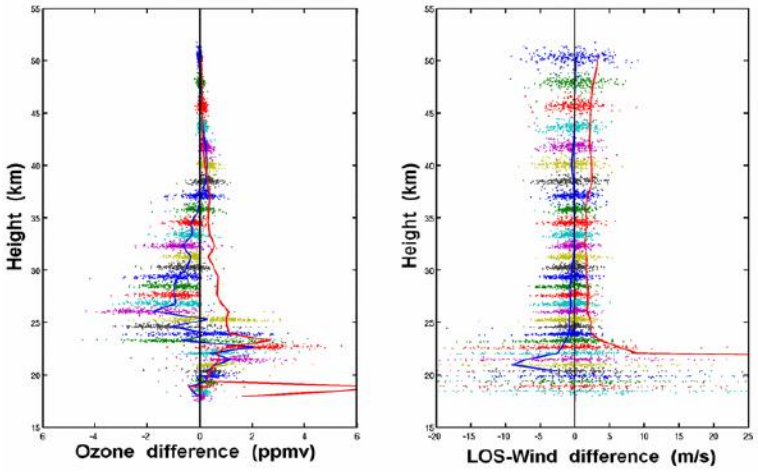

Figure 7: **On the left, residuals between the true & retrieved O_3 profiles and on the right, the residuals between the true and retrieved LOS wind using the retrieved O_3 profile. The biases (——) and standard deviations (——) are shown. The colourations of ● have the same meaning as in figure 5.**

Figure 8 illustrates the lack of effect the O_3 RT-SWIFT error has on LOS-wind retrievals by comparing individual cases. Figure 8 also illustrates the level of detail captured by the retrievals.

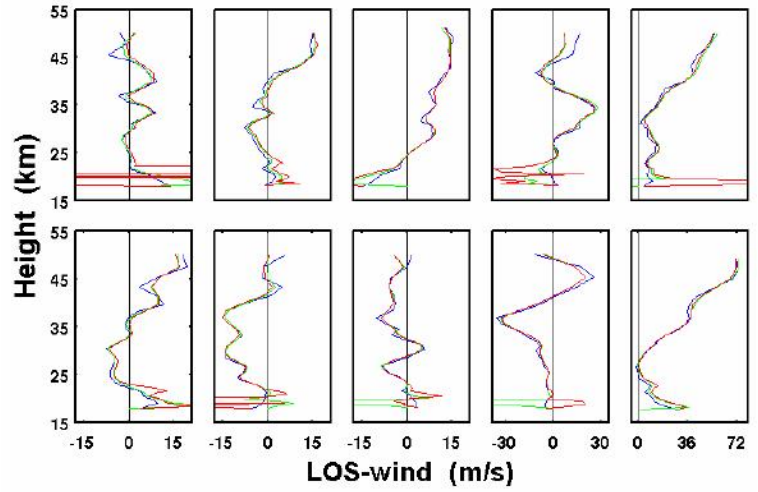

Figure 8: **Comparison of the true (——) winds, retrieved winds (——) with true O_3 and retrieved winds (——) with retrieved O_3 for a sample of 10 atmospheres chosen from the independent atmosphere set.**

CONCLUSION

The inversion results using the RT-SWIFT model generally capture the shapes of the original wind profiles with LOS wind error contributions at about 3 to 5m/s for altitudes above 24km. If a resultant 5m/s error level from other error sources is assumed, then the total retrieval error levels for SWIFT could conceivably be in the range of 6-8m/s for an effective vertical resolution of 1.5km at least up to 45km. While larger than preferred, this is still in the range of the 5-10m/s, the upper limit range for acceptable wind error levels.

While the current fast forward model yields wind error contributions larger than preferred (ie, within 1m/s), its performance suggests that effective fast forward models for Doppler measurements from instruments such as SWIFT can be devised for use in data assimilation. An investment in model performance improvements is still warranted, this being most critical for the lower levels.

REFERENCES

Bormann, N., M. Matricardi and S.B. Healy, (2005) A fast radiative-transfer model for the assimilation of infrared limb radiances from MIPAS, Quart. J. Roy. Meteor. Soc., **131**, pp1631-1653.

Lahoz, W. A., R. Brugge, D. R. Jackson, S. Migliorini, R. Swinbank, D. Lary, and A. Lee, (2005) An Observing System Simulation Experiment to evaluate the scientific merit of wind and ozone measurements from the future SWIFT instrument. Quart. J. Roy. Meteor. Soc., **131**, 502-523.

McMillin, L.M., L.J. Crone and T.J. Kleespies, (1995) Atmospheric transmittance of an absorbing gas. 5. Improvements to the OPTRAN approach, Appl. Optics, **34**, 8396-8399.

Planet, W.G., 1988: Data Extraction and Calibration of TIROS-N/NOAA Radiometers, NOAA Technical Memorandum NESS 107-Rev.1, U.S. Department of Commerce, Washington DC, 58pp.

Polavarapu, S., S. Ren, Y. Rochon, D. Sankey, N. Ek, J. Koshyk, and D. Tarasick, (2005) Data assimilation with the Canadian Middle Atmosphere Model, Atmos Ocean, **43**, pp77-100.

Rahnama, P., Y.J. Rochon, I.C. McDade, G.G. Shepherd, W.A. Gault and A. Scott, (2006) Satellite Measurement of Stratospheric Winds and Ozone Using Doppler Michelson Interferometry, Part I: Instrument Model and Measurement Simulation, J. Atmos. Ocean. Tech., **23**, pp753-769.

Rochon, Y. J., M. Keller, Y., Nezlin, R. Menard, Y.Yang, C. Haley and T.G. Shepherd, (2008) The Impact of Stratospheric Wind and Ozone Observations on Analyses and Forecasts: OSSE Description and Initial Results, Eos Trans. AGU, **89**(53), Fall Meet. Suppl., Abstract A21F-0260.

Saunders, R., M. Matricardi and A. Geer, (2008) RTTOVS9.1 Users Guide, NWP SAF Report, Met. Office, 57pp.

Shepherd, G.G.; G. Thuillier, W.A. Gault, B.H. Solheim, C. Hersom, J.M. Alunni, J.-F. Brun, S. Brune, P. Charlot, L.L. Cogger, D.-L. Desaulniers, W.F.J. Evans, R.L. Gattinger, F. Girod, D. Harvie, R.H. Hum, D.J.W. Kendall, E.J. Llewellyn, R.P. Lowe, J. Ohrt, F. Pasternak, O. Peillet, I. Powell, Y. Rochon, W.E. Ward, R.H. Wiens, J. Wimperis, (1993) WINDII, the Wind Imaging Interferometer on the Upper Atmosphere Research Satellite, J. Geophys. Res., **98**, pp 10725-10750.

Turner, D.S. and Y.J. Rochon, (2008) Towards A Fast Forward Model for Retrievals and Data Assimilation for the SWIFT Stratospheric Wind Interferometer. 37th COSPAR Scientific Assembly, Montréal, Canada.

Turner, D.S., (1995) Absorption Coefficient Estimation Using A Two Dimensional Interpolation Procedure, J. Quant. Spectrosc. Ra., **53(6)**, pp 633-637.